Wiley Online Library
Early View publication on www.wileyonlinelibrary.com
(issue and page numbers not yet assigned;
citable using Digital Object Identifier – **DOI**)

Laser Photonics Rev., 1–8 (2016) / **DOI** 10.1002/lpor.201600055

LASER & PHOTONICS REVIEWS

Abstract We reveal unusually strong polarization sensitivity of electric and magnetic dipole resonances of high-index dielectric nanoparticles placed on a metallic film. By employing dark-field spectroscopy, we observe the polarization-controlled transformation from high-Q magnetic-dipole scattering to broadband suppression of scattering associated with the electric dipole mode, and show numerically that it is accompanied by a strong enhancement of the respective fields by the nanoparticle. Our experimental data for silicon nanospheres are in an excellent agreement with both analytical calculations based on Green's function approach and the full-wave numerical simulations. Our findings further substantiate dielectric nanoparticles as strong candidates for many applications in enhanced sensing, spectroscopy and nonlinear processes at the nanoscale.

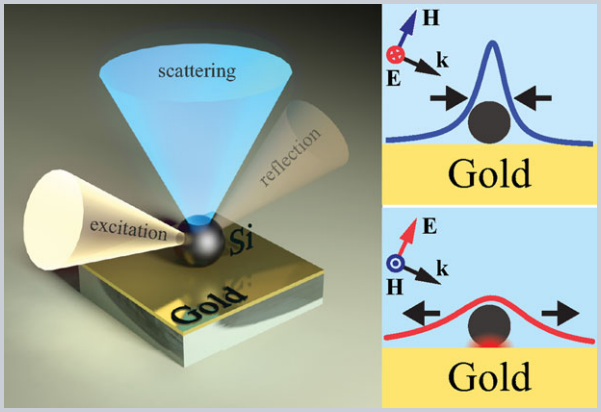

ORIGINAL PAPER

Polarization control over electric and magnetic dipole resonances of dielectric nanoparticles on metallic films

Ivan Sinev[1,*], Ivan Iorsh[1], Andrey Bogdanov[1], Dmitry Permyakov[1], Filipp Komissarenko[1,2], Ivan Mukhin[1,2], Anton Samusev[1], Vytautas Valuckas[3], Arseniy I. Kuznetsov[3], Boris S. Luk'yanchuk[3], Andrey E. Miroshnichenko[4], and Yuri S. Kivshar[1,4]

1. Introduction

Recently, high refractive index dielectric nanoparticles have attracted significant attention as a viable addition to plasmonics in the route to development of new nanophotonic devices [1–13]. The important advantages of all-dielectric over plasmonic platforms are full compatibility with complementary metal-oxide semiconductor (CMOS) technology and the presence of both magnetic and electric responses in the visible spectral range [3–5]. The interplay of these resonances has already inspired all-dielectric-based solutions for directional scatterers [9,10,14], superdirective nanoantennas [8, 15], sensors [16], metasurfaces for efficient wavefront control and beam shaping [17–20], metadevices granting a substantial enhancement of nonlinear effects [21–24], *etc.* Yet, arguably, the most important advantage of dielectric materials over metals is significanlty lower level of non-radiative losses. In particular, this leads to higher quality factor of the optical modes of nanoparticles [3,25–27] as compared to localized plasmons [28,29]. Still, high radiative losses limit the maximum Q-factor of the low-order resonances of nanoparticles, forcing to employ higher order modes for applications requiring field enhancement [25, 26, 30, 31], which means the increase of the resonator size. Therefore, an efficient way to control the quality-factor of the dipole resonances of high-index nanoparticles could open new possibilities for integration of dielectric nanoparticles in nanophotonic devices requiring compact yet effective concentrators of electromagnetic fields.

The most convenient way to manipulate the optical response of high-index nanoparticles is by changing their size and geometry [13, 17, 32–35]. Alternatively, recent studies [27, 30, 36] showed that the dielectric permittivity of the environment (*i.e.*, the substrate) also has strong impact on the optical properties of dielectric nanoparticles. Namely, low-index glass substrate was reported to reduce the scattering efficiency and Q-factors of optical resonances of high-index nanoparticles [27, 30]. Of special interest is the case of metallic substrate, which was shown to produce the enhancement of total scattering cross-section of a silicon nanosphere governed by the interaction of the electric dipole induced in the particle with its mirror image under normal excitation [36]. Furthermore, the complex interaction between the modes of the nanoparticle and the plasmonic modes of the substrate could lead to substantial modifications of the near field [37] and appearance of unusual optomechanical phenomena [38]. In particular, the recent work by Huang et al. [39] revealed strong resonant enhancement of local electric field below a silicon sphere on a metallic substrate. This effect, corroborated with the measurements of enhanced spectroscopy, was associated with

[1] ITMO University, St. Petersburg 197101, Russia
[2] St. Petersburg Academic University, St. Petersburg 194021, Russia
[3] Data Storage Institute, A*STAR (Agency for Science, Technology and Research), 138634, Singapore
[4] Nonlinear Physics Centre, Australian National University, Canberra ACT 0200, Australia
*Corresponding author: e-mail: i.sinev@metalab.ifmo.ru

the interaction of a lateral electric dipole with its mirror image generating an effective magnetic dipole response.

However, the studies of the impact of the substrate were hindered by a lack of a concise analytical model allowing to reliably address the complex problem for "particle on a surface". The solutions for this problem proposed earlier [40, 41], albeit finding their applications for modelling the near-field of low-index nanoparticles on metallic substrates [42, 43], involve laborious calculations. Thus, most of the analysis of the scattering of nanoparticles on substrates tends to be either qualitative or based on finite element methods [27, 36, 44]. A promising analytical model was proposed recently in the work by Miroshnichenko et al. [45], in which the authors unveiled the effects of substrate-induced bianisotropic interaction between electric and magnetic dipole modes of a silicon nanosphere using the approach based on Green's function. Still, the full potential of substrate as an instrument for manipulation of resonant properties of dielectric nanoparticles remains to be revealed.

In this paper, we manipulate both magnetic and electric dipole responses of a silicon nanosphere placed on a gold film by controlling the *normal* (perpendicular to the substrate surface) components sensitive to the polarization change, switching between two distinctively different effects associated with the substrate-modified response of these dipole modes. The first effect is a substantial (more than two-fold) increase of the Q-factor of optical magnetic dipole resonance that manifests itself under s-polarized oblique excitation with the resulting Q-factor of the dipole mode reaching experimental values as high as 25 and providing strong resonant enhancement of the magnetic field. The second effect is the suppression of scattering associated with the normal electric dipole component, followed by strong broadband enhancement of the electric field under the sphere.

The experimental observation of these unique effects is made possible with a custom-built dark-field microscope that allows for selective measurements of the out-of-plane electric or magnetic dipole responses of a nanoscale structure. We show that the observed effect is in perfect agreement with the predictions of analytical model for scattering from a nanoparticle on substrate [45], which allows us to analyze the impact of the substrate on each dipole component induced independently in the sphere. The demonstrated possibility of the polarization control over magnetic and electric dipole resonances of a dielectric nanoparticle enabling ample enhancement of the respective fields inspires all-dielectric-based platform for applications in enhanced sensing and spectroscopy and nonlinear processes.

2. Methods

2.1. Preparation of silicon nanospheres

The silicon nanospheres are fabricated using femtosecond laser ablation of silicon wafer and subsequent transfer onto a glass substrate. The method is described in detail elsewhere [9].

The transfer of the nanosphere from a native glass substrate to an acceptor gold film is performed via nanomanipulations under electron beam. The sample (silicon nanospheres on glass substrate) is placed in the vacuum chamber of scanning electron microscope (SEM, CrossBeam Neon 40, Carl Zeiss) along with the gold-coated substrate. The nanosphere is attached to the tip of a tapered metallic wire via dielectrophoretic and van der Waals forces and then moved to the acceptor substrate. The whole process is visualized in SEM. The method is described in more detail in Ref. [46].

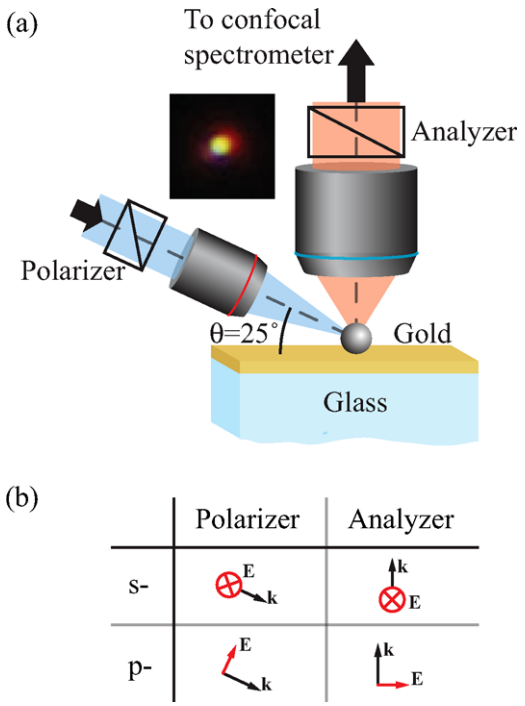

Figure 1 Polarization-resolved dark-field spectroscopy. (a) Experimental setup; a sample is excited by polarized white light at an oblique incidence. Scattered light is collected from the top by an objective with NA = 0.7 and filtered with an analyzer. The inset shows an example of a dark-field image of a 170 nm silicon nanosphere (the image size is $5 \times 5\mu m^2$). (b) Notations for the directions of polarizer and analyzer used in the paper. Each scheme shows the direction of the wave propagation and polarization of the transmitted light.

2.2. Cross-polarized dark-field spectroscopy

The detailed scheme of the dark-field spectroscopy setup is presented in Figure 1a. Linearly polarized white light (tungsten halogen source Ocean Optics HL-2000-HP) is weakly focused with an objective (Mitutoyo MPlanApo 10×, NA = 0.28) on the sample surface at oblique incidence (25° to the sample surface). The light scattered by a single particle is collected by the second objective

(Mitutoyo MPlanApo 100×, NA = 0.7) and filtered with a linear analyzer. The signal is then either analyzed with a spectrometer (Horiba LabRAM HR 800 UV-VIS-NIR) in confocal arrangement or imaged with a video camera.

2.3. Full-wave numerical simulations

Numerical simulations of the scattering spectra and fields near the nanoparticle were carried out in the frequency domain module of COMSOL Multiphysics software package. Air space surrounding the silicon nanoparticle was simulated as a half-sphere with a radius of 1 μm with the outer perfectly matched layer. The problem was solved using the scattered field formalism representing the solution as a sum of weak scattered waves (dipole radiation and SPP) and the known background field. The background field was taken as a sum of the incident, reflected, evanescent (into the gold substrate) and transmitted waves, calculated analytically from Fresnel equations.

3. Results and discussion

3.1. Experimental approach

For our studies, we use silicon nanospheres fabricated by femtosecond laser ablation of Si wafer and subsequently transferred onto a glass substrate [9]. We then place the nanospheres on a gold film (40 nm layer on top of the glass substrate) via nanomanipulations under electron beam as described in Methods section. Importantly, this technique is very delicate, and it damages neither the nanosphere nor the acceptor substrate. Note also that the thickness of the film we use exceeds the skin depth for gold in the visible spectrum, thus the film behaves nearly as a bulk substrate.

We study the scattering properties of Si nanoparticles as a function of wavelength and polarization of the incident light beam using a custom-built dark-field microscope with independent excitation (side) and collection (upper) optical channels [47, 48], Figure 1 (see also Methods section). Normally, such a setup allows to efficiently detect the scattering from in-plane (lateral) dipole modes excited in the nanoparticle [48], while using a high NA objective in the collection channel also enables more effective collection of light scattered by the normal dipole components. However, the responses of different dipole components are mixed in the detected signal.

In this study, we use a linear polarizer in the collection channel (see Figure 1). This enables us to selectively detect the scattering from the normal dipole components. Indeed, a cross-polarized analyzer (either s→p or p→s configuration, see Figure 1b) in the collection channel completely filters out the linearly polarized scattering from the induced lateral magnetic and electric dipoles. At the same time, the scattering from the normal electric and magnetic dipole components (which has radial and azimuthal polarization, respectively) is reduced only by a factor of 2 (see Section 1 of Supporting Information for details). While the possibility to selectively excite normal dipole components of a nanoparticle was recently shown by using tightly focussed cylindrical vector beams [49, 50], a dark-field setup with independent excitation and collection channels allows for selective analysis of the modes excited in a nanostructure without the need for complex polarization engineering and tight focusing, thus greatly facilitating the experimental studies of the optical properties of nanoscale systems.

The experimental results for a 170 nm silicon nanosphere are presented in Figure 2a,b which shows the dark-field scattering spectra for all four combinations of the orientations of polarizer and analyzer for glass and gold substrates, respectively. For gold substrate (Figure 2b), one can immediately see the pronounced narrow peak in the longer wavelength region for both spectra with s-polarized excitation. It can be unambiguously associated with the normal magnetic dipole response ($\mathbf{m}_z$) both due to its spectral position and the data for cross-polarized configuration (s→p, solid blue line in Figure 2), which should allow to detect only the out-of-plane dipole components. The comparison of these data with the spectra for glass substrate (Figure 2a) shows strong modification of both intensity and the quality factor of the normal magnetic dipole mode, the latter reaching an exceptional value of 25 for gold substrate. At the same time, the scattering signal for cross-polarized configuration under p-polarized excitation (p→s, Figure 1a) is extremely low, which indicates the suppression of radiation losses of $\mathbf{p}_z$ mode driven by the gold substrate.

We model the observed spectra analytically via the Green's function approach (discussed in more detail below) and numerically using finite element method (see Methods for details). In both cases we calculate the integral of Poynting vector over a spherical dome corresponding to the numerical aperture of 0.7 with account for the direction of the analyzer. The analytical and numerical spectra presented in Figure 2c,d and e,f respectively, demonstrate excellent agreement with the experimental data, accurately reproducing all spectral features for each combination of polarizer-analyzer directions both for glass and gold substrates.

3.2. Theoretical approach

To gain further insight in the observed substrate-driven modification of dipole resonances of the nanosphere, we employ the analytical approach based on Green's function suggested earlier [45]. In this model, the nanoparticle is regarded as a superposition of point electric and magnetic dipoles located at the center of the nanoparticle, and their respective polarizabilities are calculated with account for substrate-driven modifications.

Importantly, the model allows to easily retrieve the information on contributions of different components of the dipole moments induced in the nanoparticle to the scattering and extinction spectra. These contributions along with the full extinction cross-sections of a nanosphere made of

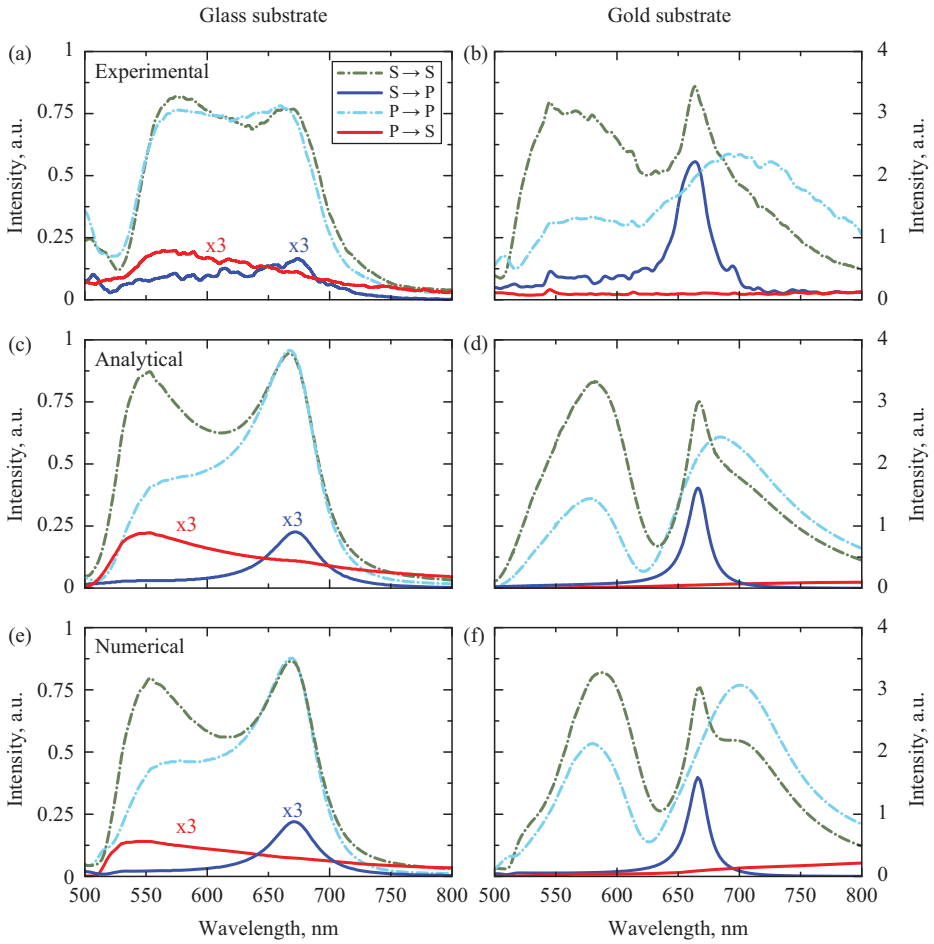

Figure 2 Scattering spectra of a silicon nanoparticle on glass and on a gold film. Top row: experimental data for a 170 nm silicon nanosphere on (a) clean glass substrate and (b) 40 nm gold film sputtered on a glass substrate. Note that the measurements were performed independently and thus the absolute values of the scattering intensities for different substrates cannot be directly compared. Middle row: Analytical results for a nanoparticle placed on a semi-infinite (c) glass and (d) gold substrate calculated via Green's function approach. Bottom row: Numerical results for silicon sphere on (e) glass and (e) 40 nm gold film obtained with the finite element method. For all panels, different curves correspond to different combinations of excitation and detected polarizations (see the scheme in Figure 1b).

crystalline silicon (diameter 170 nm) on glass (ε=2.25) and gold substrates under s- and p-polarized excitation are presented in Figure 3 (dielectric permittivity data for silicon was taken from Ref. [51], for gold - from Ref. [52)]. The full extinction cross sections of a sphere on glass substrate and their decompositions (Figure 3a, c) for both polarizations are in good agreement with previously reported results [45, 48].

The extinction cross-sections are substantially modified for the case of gold substrate. For both polarizations, the decompositions clearly show the further build-up of the effects of surface-induced bianisotropy at magnetic and electric resonances for lateral dipole components [45]. However, the dipole components that undergo the strongest modification are the normal ones. For normal magnetic dipole component, excited under s-polarized irradiation, the presence of metallic substrate leads to both drastic spectral narrowing of the resonance and an increase of its absolute scattering intensity (compare solid blue lines in Figure 3a, b). For the studied case of 170 nm silicon nanoparticle, the theoretical Q-factor is increased from 13.4 on glass to 32.7 on gold, a 2.4-fold increase. Here we recall that the experimentally measured Q-factor of the normal magnetic dipole resonance is 25, which corroborates an almost twofold enhancement as compared to theoretical limit for glass substrate. Quite contrary, the normal electric dipole, exclusive for p-polarization, experiences further broadening on gold substrate, so that its contribution to the extinction cross-section becomes non-resonant throughout the whole visible range (see Figure 3d).

3.3. Q-factor modification

The modifications of the scattering and absorption cross sections of nanoparticles driven by metallic substrates are often described in the framework of mirror images approach [29, 36, 39]. Yet, the classic mirror image theory [53, 54] inherently cannot explain the changes of the Q-factor of optical resonances since it does not imply the interaction between the system and its mirror image. As we have already shown above, such modifications are accurately predicted using the approach based on Green's function. However, this theory is not so intuitive and does not allow to immediately deduce how the substrate will affect the quality factor of the nanoparticle resonances.

Conveniently enough, it appears possible to draw qualitative predictions for the observed phenomena if we modify the mirror image theory by accounting for the interaction

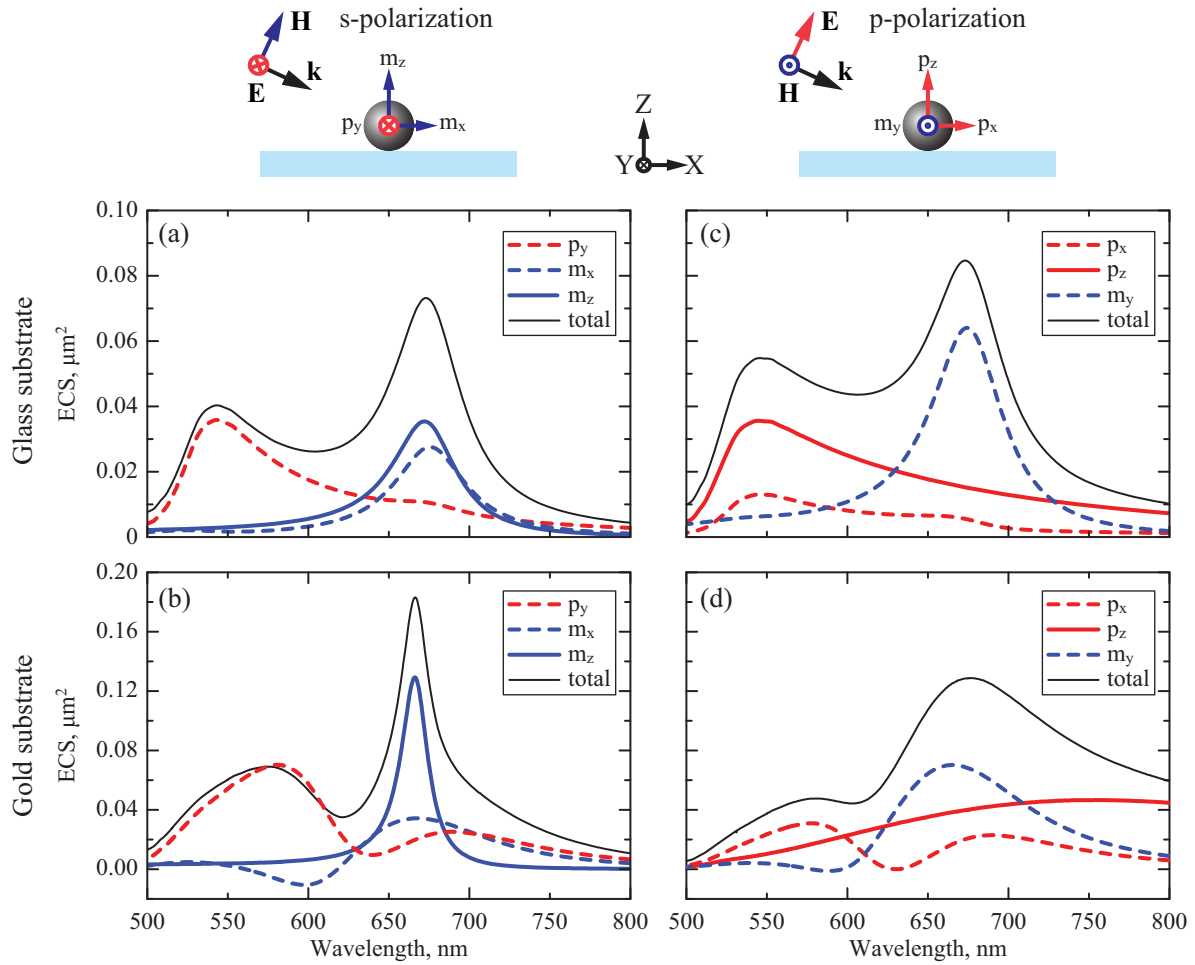

Figure 3 Total extinction cross-sections for a silicon sphere placed on glass (top row) and gold (bottom row) substrates under (a, b) s-polarized and (c, d) p-polarized excitation (angle of incidence 65°) decomposed into magnetic (blue lines) and electric (red lines) dipole contributions. Note the difference in the vertical axis scale for gold and glass substrate spectra.

between the dipole and its image. Indeed, the radiative lifetime of a system of two interacting dipoles is modified with respect to that of a single dipole and depends on the relative phase of the interacting sources (see also discussion in Section 2 of Suppoprting Information). Since both charge and current are inverted in the mirror image, the "dipole-image" pairs of normal magnetic and lateral electric moments are counteraligned, that is, out of phase (see Figure 4, top row). The interaction of anti-phase dipole sources leads to the decrease of radiative losses and, therefore, increase of the resonance Q-factor. Quite contrary, normal electric and lateral magnetic dipoles have aligned (in phase) images (see Figure 4, bottom row), which suggests increased radiation losses and, consequently, broadening of the resonance. This simple model accurately predicts the modification of the resonances Q-factor for the case of a nanosphere on perfect electric conductor (PEC) substrate. The comparison of the extinction cross-section spectra for a silicon sphere in free space and on PEC substrate can be found in Section 3 of Supporting Information.

However, a careful reader can notice that in the case of gold substrate this simple model does not provide an accurate prediction for the lateral electric dipole resonance (dashed red lines in Figure 3), which broadens instead of the anticipated pronounced spectral narrowing (see also Ref. [29] and the results for PEC substrate provided in the Supporting Information, Figure S3). This inconsistency can be explained by the dominant role of non-radiative losses. The first factor contributing to the increase of the non-radiative decay is ohmic losses, which are high due to substantial field penetration depth for gold at the frequency of electric dipole resonance of the sphere (see discussion in Section 4 of Supporting Information). The second factor is the excitation of surface plasmon polariton [38]. The same mechanisms add up to the broadening of normal electric and lateral magnetic dipole resonances predicted by the modified mirror image theory.

Normal magnetic dipole is the only component that does not suffer from the increase of non-radiative losses, since it radiates mainly along the substrate and does not couple to

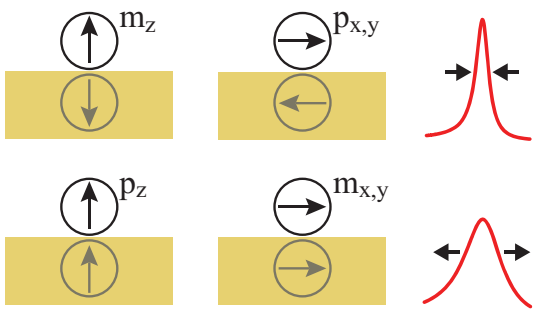

Figure 4 Schematic view of different dipole components excited in the nanoparticle and their respective mirror images induced by metal substrate illustrating the relative phase of the dipoles. In the absence of Ohmic losses, out-of-phase "dipole-image" pairs (top row) demonstrate reduced radiative losses and narrowing of the resonance, while in-phase pairs (bottom row) have increased radiative losses, which produces the broadening of the resonance.

the surface plasmon polariton mode. Therefore, its Q-factor modification is governed predominantly by the interaction with the mirror image. Careful analysis via Green's function approach shows that the extent of Q-factor modification of this resonance strongly depends on the refractive index of the sphere. Namely, it can be shown that in the limit of the large refractive index n ($\pi/n \ll 1$) the Purcell factor induced by the PEC substrate is proportional to $(\pi/n)^2$. The explicit expressions for the Purcell factor and the Lamb shift for the case of lateral and normal magnetic dipoles are presented in Section 2 of Supporting Information.

3.4. Full-wave numerical study of nanoparticle modes

Finally, we illustrate the spectral evolution of the field of the nanoparticle modes for both excitation polarizations via full-wave simulations as described in Methods section. The data for s-polarized excitation are presented in Figure 5a. The spectra of magnetic field enhancement inside the particle for both glass and gold substrates demonstrate two pronounced peaks corresponding to magnetic quadrupole and normal magnetic dipole resonances. Remarkably, the data reveal that the substrate-modified Q-factor of the magnetic dipole resonance nearly matches that of the quadrupole mode. Moreover, the magnetic dipole mode of a sphere on gold substrate becomes the one providing the best magnetic field enhancement, reaching values as high as 38.

The numerical calculations for p-polarized excitation show that the suppression of scattering cross-section of normal electric dipole is accompanied by efficient broadband localization of electric field underneath the sphere (Figure 5b). This localization is quite similar to the electric hotspot observed in a dielectric dimer [11, 13]. However, the nanosphere-on-metal system is free from technological constraints on the fabricated gap size, which limits the

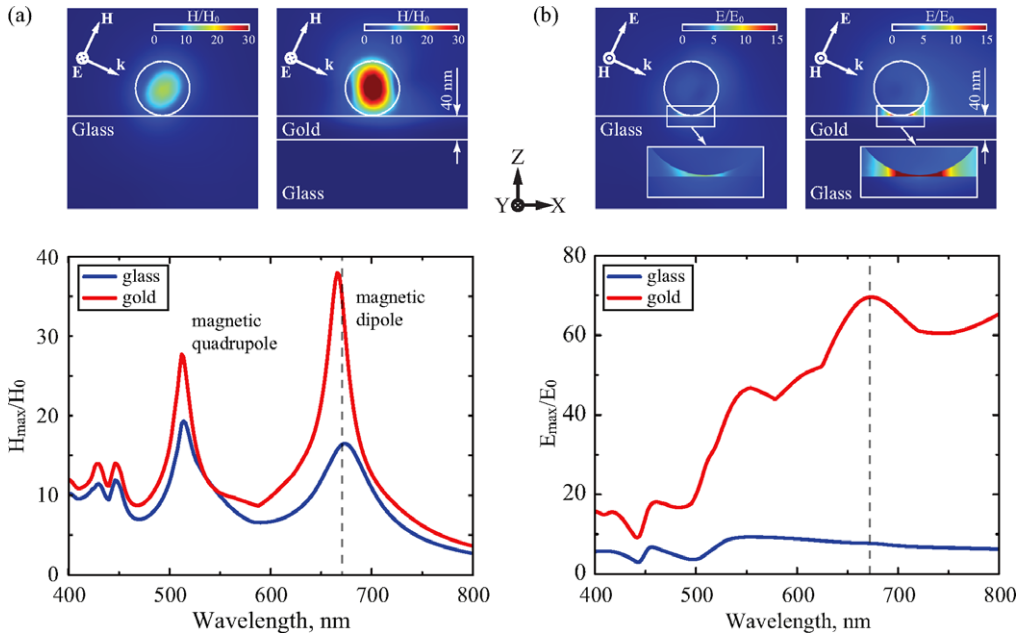

Figure 5 Numerical results for 170 nm silicon sphere on gold and glass substrates for (a) s- and (b) p-polarization. The XZ sections (top row) show the distribution of scattered electric and magnetic field amplitudes at a wavelength of 670 nm, which roughly corresponds to the wavelength of magnetic dipole resonance of the sphere. The plots in the bottom row show the spectral dependence of maximum magnetic field enhancement inside the sphere and maximum electric field enhancement in the gap below the sphere for s- and p-polarizations, respectively. 670 nm wavelength is marked with dashed lines in both plots. The gap between the nanosphere and the substrate is set to 2 nm, which corresponds to the thickness of native oxide layer on silicon [55]. The colorbars of the maps of field distribution in panels (a) and (b) are adjusted for the best visibility of the characteristic field localization.

maximum field enhancement for a silicon dimer [13]. The effective distance between the sphere and the metallic substrate is defined by the thickness of the oxide layer on the nanoparticle. In the numerical calculations, the corresponding gap was set to be 2 nm [55], which allowed for electric field enhancement of up to 70 in the visible spectral region for the given excitation geometry (Figure 5b). Most importantly, the effect of electric field localization is both strong and broadband, covering essentially all the visible spectrum. This robustness provides a significant advantage as compared to localization associated with lateral electric dipole components [39], which is resonant, thus forcing to carefully tune the size of the nanoparticles to match the wavelength for certain applications. The comparison of the electric and magnetic field enhancements at normal and oblique excitations are presented in Section 5 of Supporting Information, while the full spectral dynamics of the electric field scattered by the sphere for both polarizations under oblique excitation can be found in Supporting Information (Movies S1 and S2).

4. Conclusions and outlook

We have revealed fascinating modifications that are imposed upon normal dipole components of a high-index dielectric nanoparticle under the influence of a metallic substrate. We have shown that by controlling the polarization of the beam obliquely incident on the nanoparticle we can switch from high-Q magnetic dipole scattering to broadband suppression of scattering associated with the normal component of the electric dipole mode. We have employed cross-polarized dark-field spectroscopy which allowed for selective detection of scattering from normal electric and magnetic dipole modes induced in a nanoscale system. The experimental data for silicon spheres are in excellent agreement both with the results of analytical calculations based on Green's function approach and full-wave numerical simulations. Our study has revealed that the modifications of the Q-factor of the out-of-plane magnetic and electric dipole resonances are accompanied by a strong enhancement of the respective fields by the nanoparticle. These properties call for further expansion of the scope of applications of high-index dielectric nanoparticles, suggesting new ideas for sensing and enhancement of nonlinear processes.

Supporting Information

Additional supporting information may be found in the online version of this article at the publisher's website.

Acknowledgements. Experimental part of the work, including the transfer of the nanoparticle to metallic substrate and the optical measurements as well as numerical and analytical simulations carried out at ITMO University were financially supported by Russian Science Foundation (grant #15-12-20028). The authors at ANU were supported by the Australian Research Council. The authors at DSI were supported by DSI core funds and A*STAR SERC Pharos program, Grant 152 73 00025 (Singapore). We are grateful to Andrey B. Evlyukhin and Alexander E. Krasnok for fruitful discussions and comments.

Received: 29 February 2016, **Revised:** 28 June 2016, **Accepted:** 5 July 2016

Published online: 4 August 2016

Key words: dielectic nanoparticles, magnetic dipole resonance, dark-field spectroscopy, electromagnetic field localization.

References

[1] A. B. Evlyukhin, C. Reinhardt, A. Seidel, B. S. Luk'yanchuk, and B. N. Chichkov, Phys. Rev. B **82**(4), 45404 (2010).
[2] A. García-Etxarri, R. Gómez-Medina, L. S. Froufe-Pérez, C. López, L. Chantada, F. Scheffold, J. Aizpurua, M. Nieto-Vesperinas, and J. J. Sáenz, Opt. Express **19**(6), 4815–4826 (2011).
[3] A. I. Kuznetsov, A. E. Miroshnichenko, Y. H. Fu, J. Zhang, and B. Luk'yanchuk, Sci. Rep. **2**, 492 (2012).
[4] A. B. Evlyukhin, S. M. Novikov, U. Zywietz, R. L. Eriksen, C. Reinhardt, S. I. Bozhevolnyi, and B. N. Chichkov, Nano Lett. **12**(7), 3749–3755 (2012).
[5] L. Shi, T. U. Tuzer, R. Fenollosa, and F. Meseguer, Adv. Mater. **24**(44), 5934–5938 (2012).
[6] A. E. Miroshnichenko and Y. S. Kivshar, Nano Lett. **12**(12), 6459–6463 (2012).
[7] M. K. Schmidt, R. Esteban, J. Sáenz, I. Suárez-Lacalle, S. Mackowski, and J. Aizpurua, Opt. Express **20**(13), 13636–13650 (2012).
[8] A. E. Krasnok, A. E. Miroshnichenko, P. A. Belov, and Y. S. Kivshar, Opt. Express **20**(18), 20599–20604 (2012).
[9] Y. H. Fu, A. I. Kuznetsov, A. E. Miroshnichenko, Y. F. Yu, and B. Luk'yanchuk, Nat. Commun. **4**, 1527 (2013).
[10] S. Person, M. Jain, Z. Lapin, J. J. Sáenz, G. Wicks, and L. Novotny, Nano Lett. **13**(4), 1806–1809 (2013).
[11] P. Albella, M. A. Poyli, M. K. Schmidt, S. A. Maier, F. Moreno, J. J. Sáenz, and J. Aizpurua, J. Phys. Chem. C **117**(26), 13573–13584 (2013).
[12] B. S. Luk'yanchuk, N. V. Voshchinnikov, R. Paniagua-Dom' inguez, and A. I. Kuznetsov, ACS Photonics **2**(7), 993–999 (2015).
[13] R. M. Bakker, D. Permyakov, Y. F. Yu, D. Markovich, R. Paniagua-Domínguez, L. Gonzaga, A. Samusev, Y. S. Kivshar, B. Luk'yanchuk, and A. I. Kuznetsov, Nano Lett. **15**(3), 2137–2142 (2015).
[14] I. Staude, A. E. Miroshnichenko, M. Decker, N. T. Fofang, S. Liu, E. Gonzales, J. Dominguez, T. S. Luk, D. N. Neshev, I. Brener, and Others, ACS Nano **7**(9), 7824–7832 (2013).
[15] A. E. Krasnok, C. R. Simovski, P. A. Belov, and Y. S. Kivshar, Nanoscale **6**(13), 7354–7361 (2014).
[16] M. Caldarola, P. Albella, E. Cortes, M. Rahmani, T. Roschuk, G. Grinblat, R. F. Oulton, A. V. Bragas, and S. A. Maier, Nat. Commun. **6**, (2015).
[17] M. Decker, I. Staude, M. Falkner, J. Dominguez, D. N. Neshev, I. Brener, T. Pertsch, and Y. S. Kivshar, Adv. Opt. Mater. **3**(6), 813–820 (2015).

[18] Y. F. Yu, A. Y. Zhu, R. Paniagua-Domínguez, Y. H. Fu, B. Luk'yanchuk, and A. I. Kuznetsov, Laser Photonics Rev. **9**(4), 412–418 (2015).
[19] K. E. Chong, I. Staude, A. James, J. Dominguez, S. Liu, S. Campione, G. S. Subramania, T. S. Luk, M. Decker, D. N. Neshev, I. Brener, and Y. S. Kivshar, Nano Lett. **15**(8), 5369–5374 (2015).
[20] M. I. Shalaev, J. Sun, A. Tsukernik, A. Pandey, K. Nikolskiy, and N. M. Litchinitser, Nano Lett. **15**(9), 6261–6266 (2015).
[21] M. R. Shcherbakov, D. N. Neshev, B. Hopkins, A. S. Shorokhov, I. Staude, E. V. Melik-Gaykazyan, M. Decker, A. A. Ezhov, A. E. Miroshnichenko, I. Brener, A. A. Fedyanin, and Y. S. Kivshar, Nano Lett. **14**(11), 6488–6492 (2014).
[22] S. Makarov, S. Kudryashov, I. Mukhin, A. Mozharov, V. Milichko, A. Krasnok, and P. Belov, Nano Lett. **15**(9), 6187–6192 (2015).
[23] M. R. Shcherbakov, P. P. Vabishchevich, A. S. Shorokhov, K. E. Chong, D. Y. Choi, I. Staude, A. E. Miroshnichenko, D. N. Neshev, A. A. Fedyanin, and Y. S. Kivshar, Nano Lett. **15**(10), 6985–6990 (2015).
[24] Y. Yang, W. Wang, A. Boulesbaa, I. I. Kravchenko, D. P. Briggs, A. Puretzky, D. Geohegan, and J. Valentine, Nano Lett. **15**(11), 7388–7393 (2015).
[25] R. Fenollosa, F. Meseguer, and M. Tymczenko, Advanced Materials **20**(1), 95–98 (2008).
[26] E. Xifré-Pérez, R. Fenollosa, and F. Meseguer, Opt. Express **19**(4), 3455–3463 (2011).
[27] D. L. Markovich, P. Ginzburg, A. K. Samusev, P. A. Belov, and A. V. Zayats, Opt. Express **22**(9), 10693–10702 (2014).
[28] M. B. Ross and G. C. Schatz, J. Phys. D: Appl. Phys. **48**(18), 184004 (2015).
[29] A. Sobhani, A. Manjavacas, Y. Cao, M. J. McClain, F. J. G. de Abajo, P. Nordlander, and N. J. Halas, Nano Lett. **15**(10), 6946–6951 (2015).
[30] L. Shi, R. Fenollosa, T. U. Tuzer, and F. Meseguer, ACS Photonics **1**(5), 408–412 (2014).
[31] I. Rodriguez, L. Shi, X. Lu, B. Korgel, R. Alvarez-Puebla, and F. Meseguer, Nanoscale **6**(11), 5666–5670 (2014).
[32] A. B. Evlyukhin, C. Reinhardt, and B. N. Chichkov, Phys. Rev. B **84**, 235429 (2011).
[33] A. B. Evlyukhin, C. Reinhardt, E. Evlyukhin, and B. N. Chichkov, J. Opt. Soc. Am. B **30**(10), 2589–2598 (2013).
[34] U. Zywietz, M. K. Schmidt, A. B. Evlyukhin, C. Reinhardt, J. Aizpurua, and B. N. Chichkov, ACS Photonics **2**(7), 913–920 (2015).
[35] A. E. Miroshnichenko, A. B. Evlyukhin, Y. F. Yu, R. M. Bakker, A. Chipouline, A. I. Kuznetsov, B. Luk'yanchuk, B. N. Chichkov, and Y. S. Kivshar, Nat. Commun. **6**, (2015).
[36] E. Xifré-Pérez, L. Shi, U. Tuzer, R. Fenollosa, F. Ramiro-Manzano, R. Quidant, and F. Meseguer, ACS Nano **7**(1), 664–668 (2012).
[37] T. Hutter, F. M. Huang, S. R. Elliott, and S. Mahajan, J. Phys. Chem. C **117**(15), 7784–7790 (2013).
[38] M. I. Petrov, S. V. Sukhov, A. A. Bogdanov, A. S. Shalin, and A. Dogariu, Laser Photonics Rev. **10**(1), 116–122 (2016).
[39] Z. Huang, J. Wang, Z. Liu, G. Xu, Y. Fan, H. Zhong, B. Cao, C. Wang, and K. Xu, J. Phys. Chem. C **119**(50), 28127–28135 (2015).
[40] P. A. Bobbert and J. Vlieger, Physica A **137**(1), 209–242 (1986).
[41] G. Videen, J. Opt. Soc. Am. A **10**(1), 110–117 (1993).
[42] B. S. Luk'yanchuk, Y. W. Zheng, and Y. Lu, Proc. SPIE **4065**, 576–587 (2000).
[43] S. Huang, M. Hong, B. Luk'yanchuk, Y. Zheng, W. Song, Y. Lu, and T. Chong, J. Appl. Phys **92**(5), 2495–2500 (2002).
[44] F. Bernal Arango, T. Coenen, and A. F. Koenderink, ACS Photonics **1**(5), 444–453 (2014).
[45] A. E. Miroshnichenko, A. B. Evlyukhin, Y. S. Kivshar, and B. N. Chichkov, ACS Photonics **2**(10), 1423–1428 (2015).
[46] A. I. Denisyuk, F. E. Komissarenko, and I. S. Mukhin, Microelectron. Eng. **121**, 15–18 (2014).
[47] J. A. Fan, C. Wu, K. Bao, J. Bao, R. Bardhan, N. J. Halas, V. N. Manoharan, P. Nordlander, G. Shvets, and F. Capasso, science **328**(5982), 1135–1138 (2010).
[48] D. Permyakov, I. Sinev, D. Markovich, P. Ginzburg, A. Samusev, P. Belov, V. Valuckas, A. I. Kuznetsov, B. S. Luk'yanchuk, A. E. Miroshnichenko, D. N. Neshev, and Y. S. Kivshar, Appl. Phys. Lett. **106**(17), 171110 (2015).
[49] P. Banzer, U. Peschel, S. Quabis, and G. Leuchs, Opt. Express **18**(10), 10905–10923 (2010).
[50] P. Woźniak, P. Banzer, and G. Leuchs, Laser Photonics Rev. **9**(2), 231–240 (2015).
[51] E. D. Palik, Handbook of optical constants of solids (Academic press, 1997).
[52] A. D. Rakić, A. B. Djurišić, J. M. Elazar, and M. L. Majewski, Appl. Optics **37**(22), 5271–5283 (1998).
[53] J. D. Jackson, Classical electrodynamics, third edition (Wiley, New York, 1998).
[54] L. Novotny and B. Hecht, Principles of nano-optics (Cambridge university press, 2012).
[55] M. Morita, T. Ohmi, E. Hasegawa, M. Kawakami, and M. Ohwada, J. Appl. Phys. **68**(3), 1272–1281 (1990).

Supporting Information

Polarization control over electric and magnetic dipole resonances of dielectric nanoparticles on metallic films

Ivan Sinev,[*,†] Ivan Iorsh,[†] Andrey Bogdanov,[†] Dmitry Permyakov,[†] Filipp Komissarenko,[†] Ivan Mukhin,[†,‡] Anton Samusev,[†] Vytautas Valuckas,[¶] Arseniy I. Kuznetsov,[¶] Boris S. Luk'yanchuk,[¶] Andrey E. Miroshnichenko,[§] and Yuri S. Kivshar[†,§]

†*ITMO University, St. Petersburg 197101, Russia*

‡*St. Petersburg Academic University, St. Petersburg 194021, Russia*

¶*Data Storage Institute, A*STAR (Agency for Science, Technology and Research), 138634, Singapore*

§*Nonlinear Physics Centre, Australian National University, Canberra ACT 0200, Australia*

E-mail: i.sinev@metalab.ifmo.ru

1. Selective measurements of dipole responses of nanoparticles with cross-polarized dark-field spectroscopy

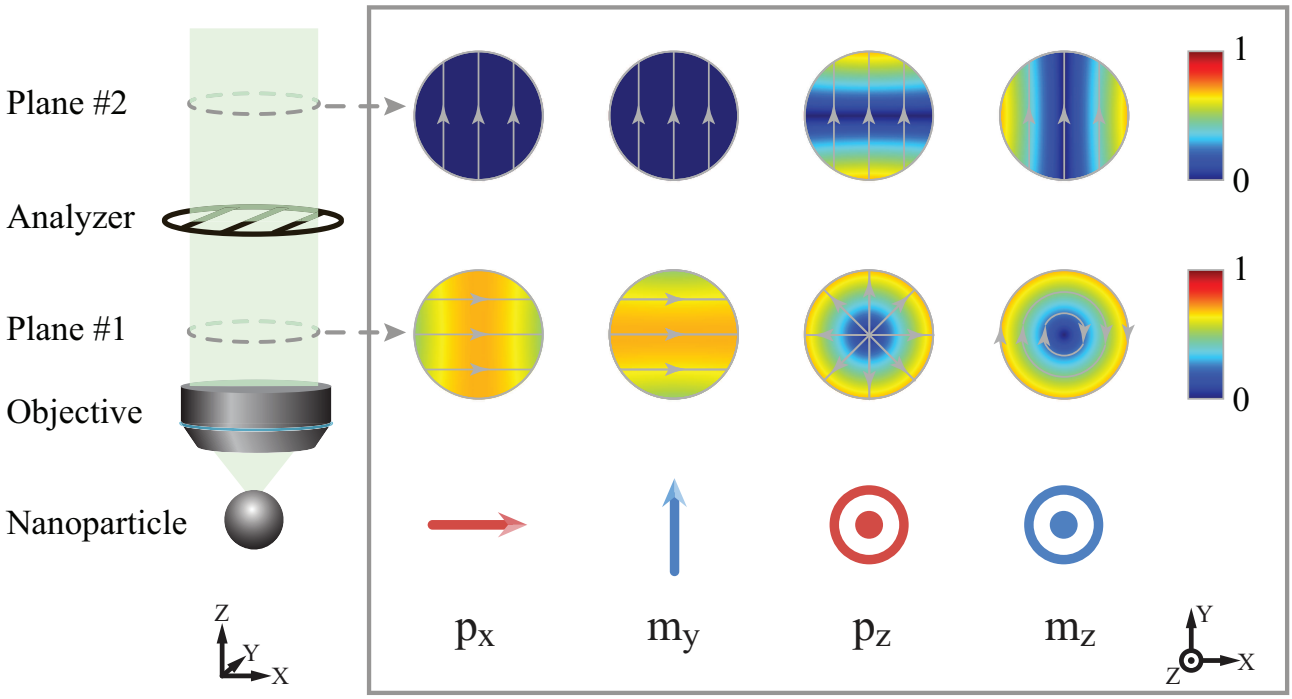

Figure S1: The illustration for the principle of operation of cross-polarized dark-field spectroscopy setup. The scheme on the left shows the collection channel of the polarization-resolved dark-field microscope (see also Figure 1 in the main text) measuring the scattering from a single silicon nanoparticle. The linear analyzer in the collection channel transmits the light polarized along the y axis. The inset on the right shows the analytically calculated distributions of the electric field amplitude in the k-space (back focal plane images of the infinity-corrected collection objective) induced by scattering from different dipole components of the nanosphere. The bottom and top row images show the distributions before (Plane #1) and after (Plane #2) the light is filtered with the analyzer, respectively. The polarization directions are shown with grey arrows in each image.

In this section, we illustrate the principle of operation of cross-polarized dark-field microscope described in the main text. The light scattered by lateral electric and magnetic dipole components of the nanosphere (either p_x or m_y, first two columns in Figure S1) is linearly polarized and is thus completely filtered by the analyzer in the collection channel. Quite contrary, the scattering collected from *normal* dipole components of the nanosphere is polarized either radially (for electric dipole p_z, third column in Figure S1) or azimuthally (for magnetic dipole

m_z, last column in Figure S1). Therefore, after the analyzer the integral signal is modified only by a factor of 2, allowing to selectively detect the scattering from normal dipole components of the nanoparticle.

2. Magnetic dipole response of a sphere above perfect electric conductor

Let us consider analytically the modification of magnetic dipole response of a high index dielectric sphere placed above a perfect electric conductor. Note that not unlike the mirror image theory, the problem of the plane wave scattering by a dipole placed over the perfectly conducting plane maps directly to the problem of the plane wave scattered by a system of two dipoles, where the second (auxiliary) dipole is polarized only by a field scattered from the first dipole and is not polarized by the incident field.

We start from the general expression for the magnetic dipole cross-section:

$$\sigma_m = \frac{\omega}{2P_{in}}\mathrm{Im}(\mathbf{m}\mathbf{H}_0^*), \tag{1}$$

where P_{in} is the incident power and $\mathbf{m}$ is the magnetic dipole polarization, and H_0 is the full magnetic field at the point of the dipole, which in the case of TE polarization is given by:

$$\mathbf{H}_0 = [\cos\alpha(1+\exp[2ik_0R\cos\alpha]), 0, \sin\alpha(1-\exp[2ik_0R\cos\alpha])], \tag{2}$$

where α is the angle of incidence.

Recalling that $\mathbf{m} = \alpha_{hh}\mathbf{H}_0$, we can rewrite:

$$\sigma_m = 4k_0\mathbf{Im}\left(\alpha_{hh,xx}\cos^2\alpha\cos^2(k_0R/\cos\alpha) + \alpha_{hh,zz}\sin^2\alpha\sin^2(k_0R/\cos\alpha)\right). \tag{3}$$

We can now consider each term of the Eq. (3) separately. The z component is given by:

$$\alpha_{hh,zz} = \frac{\alpha_h}{1 - \alpha_h G_{hh,zz}}, \tag{4}$$

where $G_{hh,zz}$ is the zz component of the reflection part of the Green's function which reads

$$G_{hh,zz} = -\frac{i}{4\pi} k_0^3 \int_0^\infty \frac{x^3}{\sqrt{1-x^2}} e^{2i\sqrt{1-x^2}k_0 R} dx = \frac{e^{2ik_0 R}(2ik_0 R - 1)}{16\pi R^3}, \tag{5}$$

and α_h is the bare polarizability of the dielectric sphere, $\alpha_h = -6\pi i/k_0^3 b_1$, where b_1 is the Mie coefficient which can be expanded in the vicinity of the resonance as:

$$b_1 \approx \frac{-i\gamma_h}{(\omega - \omega_h) + i\gamma_h}, \tag{6}$$

where ω_h is the dipole resonance, and γ_h is the peak width. Rewriting the expression for polarizability we get:

$$\alpha_h = -\frac{6\pi}{k_0^3} \frac{\gamma_h}{(\omega - \omega_h) + i\gamma_h} \tag{7}$$

We then assume that the Green's function changes slowly in the vicinity of the magnetic resonance and we substitute $k_0 R \to k_h R \approx \pi/n$, where k_h is the wavevector corresponding to the magnetic dipole resonance and n is the sphere refractive index. The expression for the dressed polarizability is then given by:

$$\alpha_{hh,zz} \approx \frac{-6\pi/k_0^3 \gamma_h}{\omega - \omega_h + i\gamma_h + \gamma_h \frac{3}{8(\pi/n)^3} e^{2i\pi/n}(2i\pi/n - 1)}. \tag{8}$$

The above expression can be rewritten as

$$\alpha_{hh,zz} \approx \frac{-6\pi/k_0^3 \gamma_h}{\omega - \tilde{\omega_h} + i\tilde{\gamma_h}}, \tag{9}$$

where

$$\tilde{\omega}_h = \omega_h \left(1 + \frac{3}{Q}\frac{\cos(2\pi/n) + (2\pi/n)\sin(2\pi/n)}{(2\pi/n)^3}\right), \tag{10}$$

$$\tilde{\gamma}_h = \gamma_h \left(1 - 3\frac{\sin(2\pi/n) - (2\pi/n)\cos(2\pi/n)}{(2\pi/n)^3}\right), \tag{11}$$

where $Q = \omega_h/\gamma_h$ is the quality factor of magnetic dipole resonance. In the limit $\pi/n \ll 1$ the expression can be simplified to

$$\tilde{\omega}_h = \omega_h \left(1 + \frac{3}{Q(2\pi/n)^3}\right), \tag{12}$$

$$\tilde{\gamma}_h = \frac{\gamma_h}{10}\left(\frac{2\pi}{n}\right)^2 \tag{13}$$

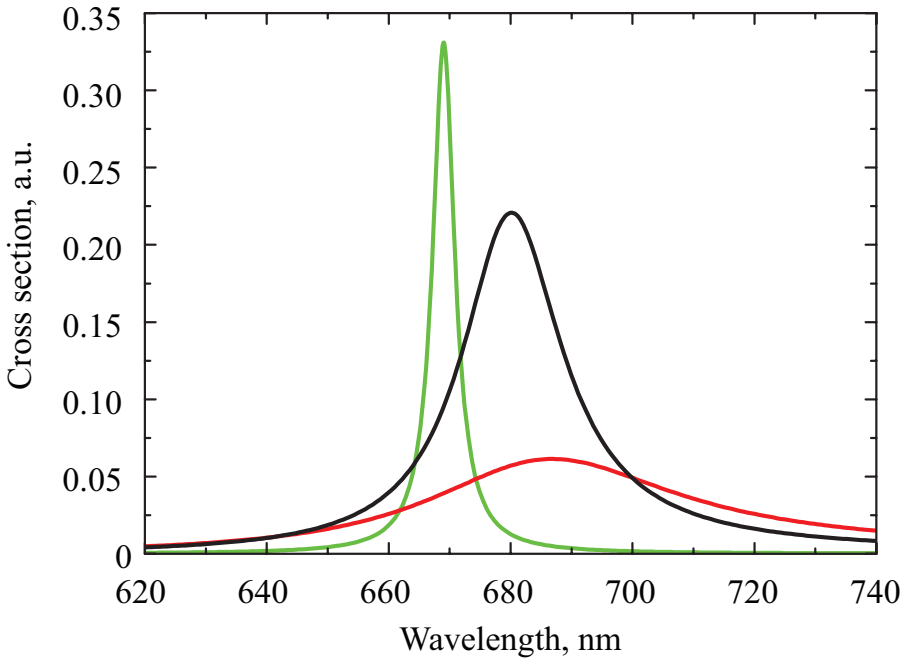

Figure S2: Scattering cross-sections of the magnetic dipole in vacuum (black line), z component over PEC (green line) and x component over PEC (red line)

For the case of x-polarized dipole the procedure is fully analogous up to the picking another

component of the Green's function which we introduce as:

$$G_{hh,xx} = \frac{e^{2ik_0R}(2ik_0R - 1 + 4k_0^2R^2)}{32\pi R^3}. \tag{14}$$

Substituting $k_0R \to k_hR \approx \pi/n$, gives us expressions for the dressed resonance frequency and linewidth:

$$\tilde{\omega}_h = \omega_h \left(1 + \frac{3}{2Q}\frac{\cos(2\pi/n)(1-(2\pi/n)^2) + (2\pi/n)\sin(2\pi/n)}{(2\pi/n)^3}\right), \tag{15}$$

$$\tilde{\gamma}_h = \gamma_h \left(1 - \frac{3}{2}\frac{\sin(2\pi/n)(1-(2\pi/n)^2) - (2\pi/n)\cos(2\pi/n)}{(2\pi/n)^3}\right). \tag{16}$$

These expressions can also be simplified for the case of large refractive index $2\pi/n \ll 1$:

$$\tilde{\omega}_h = \omega_h \left(1 - \frac{3}{Q(2\pi/n)^3}\right), \tag{17}$$

$$\tilde{\gamma}_h = \gamma_h \left(2 - (2\pi/n)^2/5\right) \tag{18}$$

The plot of the scattering cross sections for a magnetic dipole in vacuum, x component of the dipole over PEC and z component of the dipole over PEC are shown in Figure S2.

3. Scattering from a sphere in free space and on perfect electric conductor substrate

We compare the predictions of mirror image approach (see Figure 4 in the main text) for the metal substrate-driven modifications of the Q-factor of magnetic and electric dipole modes with the results of the analytical model. Figure S3 shows the comparison of extinction cross section (ECS) spectra of different dipole components calculated via Green's function approach for a sphere in free space and on PEC substrate (PEC is modelled with a permittivity of $-0.1 + 100000i$ for all wavelengths). In full agreement with the predictions of the modified

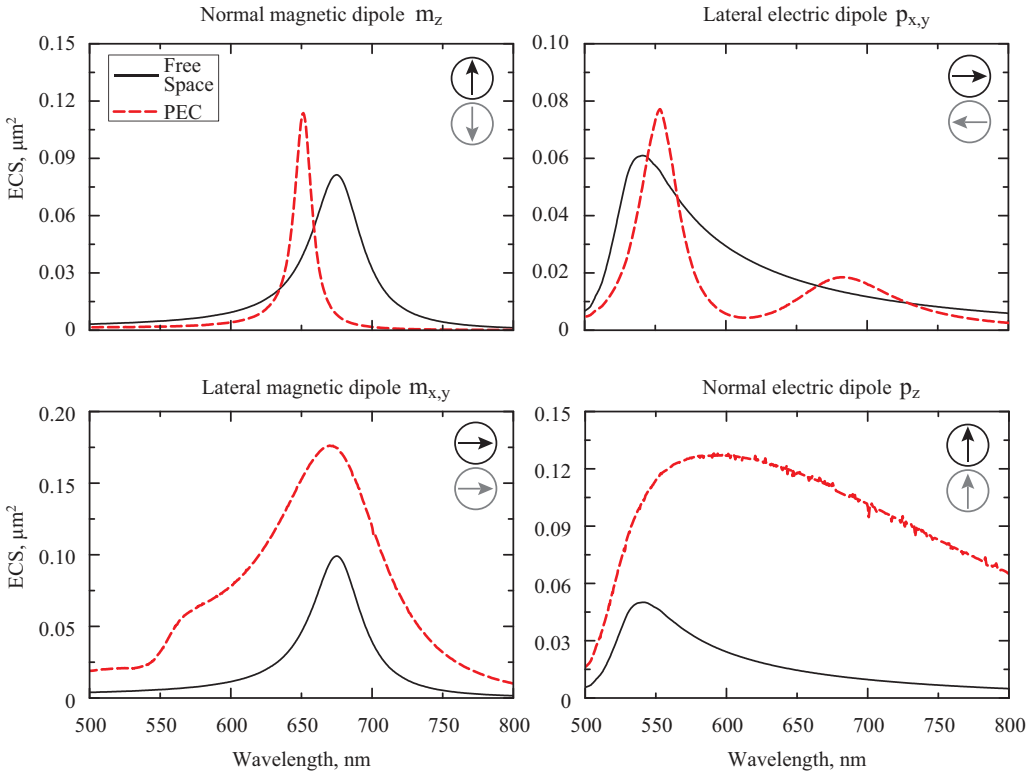

Figure S3: Comparison of the extinction cross sections from different components of electric and magnetic dipoles induced in a 170 nm silicon sphere in free space (solid black lines) and on PEC substrate (dashed red lines). The size of the silicon sphere and the excitation geometry correspond to those discussed in the main text. The insets in each plot show the scheme of the corresponding dipole and its respective mirror image induced by PEC substrate.

mirror image approach, the spectra show the narrowing of normal magnetic and lateral electric dipole resonances and the broadening of lateral magnetic and normal electric dipole modes for the case of PEC substrate as compared to free space. This demonstrates good applicability of the modified mirror image approach for qualitative predictions for scattering from a dielectric particle on metal in the absence of Ohmic losses.

4. Influence of non-radiative losses on the substrate-induced modification of dipole resonances

We study the influence of the level of non-radiative losses on the extinction spectra using lateral electric dipole as an example. Figure S4 shows the comparison of ECS from lateral electric

dipole component of the silicon sphere in free space and on different metallic substrates: PEC, gold and aluminium (The dielectric permittivity data is taken from Ref. 1). The spectra clearly show the spectral narrowing of the resonance for aluminium and PEC substrate, while there is no pronounced narrowing for gold substrate, which is due to higher level of absorption by gold. Indeed, while the imaginary part of dielectric permittivity is higher for aluminium (12.3 versus 1.9 for gold at 550 nm), the field penetration depth defined by the wave impedance of the material is much higher for gold due to huge absolute value of the real part of permittivity (-5.3 versus -40 for aluminium at the same wavelength).[1] Thus, the absorption is higher for gold, which leads to loss-driven broadening of the lateral electric dipole resonance "overriding" the narrowing mechanisms.

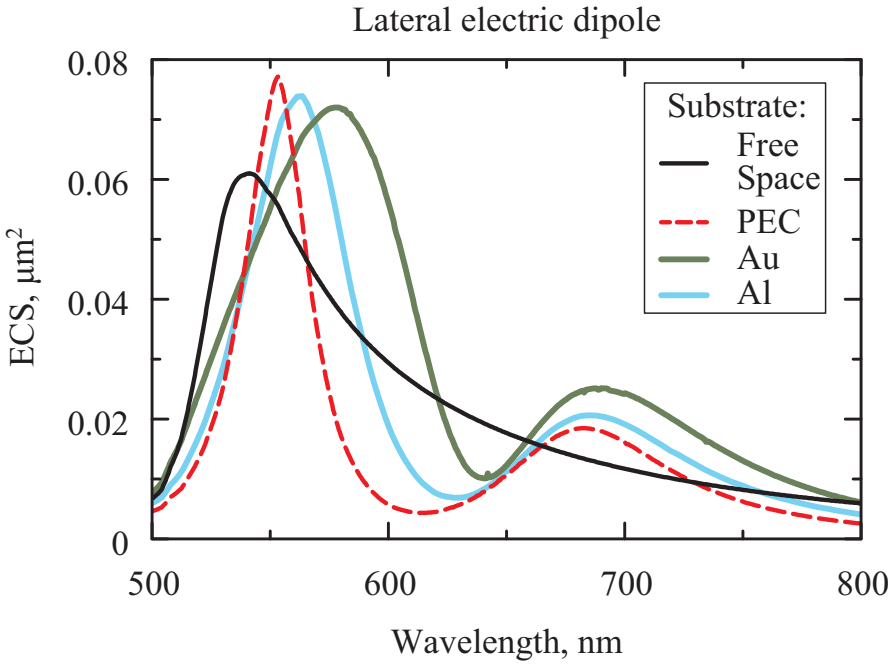

Figure S4: Comparison of the extinction cross sections of lateral electric dipole component of 170 nm silicon nanosphere in free space and on Al, Au, and PEC substrates.

5. Field enhancement by silicon nanosphere on gold at normal and oblique excitation

Here, we compare the potency of field localization by a silicon nanosphere on gold excited at either oblique or normal incidence. The key difference is that while linearly polarized light at normal incidence is only capable of generating lateral dipole response from the nanosphere, obliquely incident beam can also induce electric and magnetic dipole components of the nanosphere which are normal to the substrate. The results of numerical calculation of the maximum magnetic field inside the sphere and the maximum electric field in the gap between the sphere and the gold substrate for these two geometries are summarized in Figure S5. It unambiguously shows the advantages of utilizing normal magnetic and electric dipole modes of a nanosphere on gold substrate for achieving maximum local concentration of the respective fields.

For s-polarization of the obliquely incident beam, the substrate-driven modification of the magnetic dipole resonance Q-factor provides eminently better resonant magnetic field enhancement, which reaches a value of 38 as compared to a moderate maximum of 20 for normal excitation (Figure S5 a). As for the electric field enhancement (Figure S5 b), in the considered case of 170 nm silicon nanosphere the normally incident beam provides a competitive maxi-

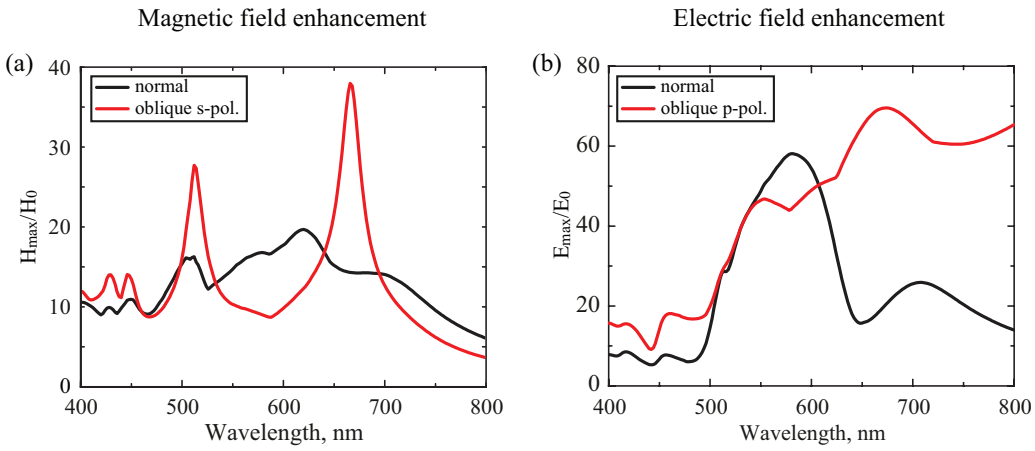

Figure S5: Comparison of the enhancement of (a) magnetic and (b) electric fields by a 170 nm silicon nanosphere on gold substrate for normal (black lines) and oblique (angle of incidence 65°, red lines) excitation geometries.

mum electric field enhancement of 60, corresponding to effective magnetic dipole generated by substrate-driven modification of lateral electric dipole resonance of the sphere.[2] However, it is not as strong and not nearly as broadband as the enhancement provided by the normal electric dipole mode of the nanoparticle induced for p-polarized oblique excitation, which essentially covers all the visible spectrum. This robust enhancement greatly facilitates the application of silicon nanoparticles for enhanced sensing and spectroscopy, since the effect provided is both strong and extremely broadband.

Captions for movies S1 and S2

Movie S1 Spectral dependence of the distribution of the amplitude of magnetic field scattered by a 170 nm silicon sphere on 40 nm gold film in the plane of incidence for s-polarized excitation. The counter shows the maximum electric field amplification within the section for the current wavelength normalized by the amplitude of electric field in the incident wave. The calculated spectral dependence of scattering signal for a collection objective with a numerical aperture of 0.7 is shown on the right.

Movie S2 Spectral dependence of the distribution of the amplitude of electric field scattered by a 170 nm silicon sphere on 40 nm gold film for p-polarized excitation. The counter shows the maximum electric field amplitude within the section for the current wavelength normalized by the amplitude of electric field in the incident wave. The plot on the right shows the full spectral dependence of the maximum electric field enhancement.

References

(1) A.D. Rakić, A.B. Djurišić, J.M. Elazar, and M.L. Majewski, "Optical Properties of Metallic Films for Vertical-Cavity Optoelectronic Devices," Appl. Optics **37**, 5271 (1998)

(2) Z. Huang, J. Wang, Z. Liu, G. Xu, Y. Fan, H. Zhong, B. Cao, C. Wang, and K. Xu,

"Strong-Field-Enhanced Spectroscopy in Silicon Nanoparticle Electric and Magnetic Dipole Resonance near a Metal Surface," J. Phys. Chem. C **119**, 28127 (2015)